Analytical Model for Optically Generated Currents in GaAs MESFETs

Asher Madjar, *Senior Member IEEE,* Peter R. Herczfeld, *Fellow, IEEE,* and Arthur Paolella

***Abstract*—The MESFET as an optically sensitive microwave element on MMIC's has attracted much attention. The theoretical modelling of the device, however, needs more consideration. This paper proposes an analytical model for the illuminated MESFET, complete in that all major contributions to the optical response are considered. The dependence of the response on bias conditions, the wavelength and intensity of the optical input, and the particulars of device structure, are incorporated in the model. The importance of the internal photovoltaic effect, which has not been properly modelled previously, is emphasized. The novel theoretical model is verified by experimental results.**

Nomenclature

λ, α, P_{opt}	Wavelength, absorption coefficient and power density per unit area of incident light.
$F = T_r P_{opt}/h\nu$ $= T_r \lambda P_{opt}/hc$	Absorbed photon flux per unit area per unit time.
T_r	Optical transmission coefficient via the passivation layer (silicon nitride).
q, h, c	Electron charge, Plack's constant, velocity of light in vacuum.
n_e, n_s	Dark electron concentration in the epi layer and substrate.
n, p	Optically generated excess electron and hole distributions.
D_n, μ_n, τ_n, L_n	Diffusion coefficient, mobility, lifetime, diffusion length for electrons (and holes $n >> p$).
$\tau_{tn} = L/v_n$	Electron (and hole $n >> p$) transit time in the effective illuminated channel on the drain side.
$G_n = \tau_n/\tau_{tn}$	Electron (and hole $n >> p$) photoconductive gain in channel.
μ_s	Electron mobility in the substrate.
v_s, v_{pk}	Saturated velocity ($\sim 10^7$ cm/sec), and peak velocity.
E_c, E_{sp}	Critical electric fields for velocity saturation (electrons, holes).
a, a_e, l_{sub}	Epi layer thickness (recessed and unrecessed) and substrate thickness.
h_{cd}, h_{cs}	Channel height on drain side and source side.
h_T, h_s	Gate depletion region height.
$A_{dL} = wL$, $A_{sL} = wh_s$	Effective illuminated areas (w = gate width, L and h_s are gate depletion extensions beyond metallization on drain and source sides).
$A_{leak} = w_s d$	Leakage effective illuminated area (w_s = width of electrodes in close proximity, d = depletion length).
$A_d = wl_{gd}$, $A_s = wl_{gs}$	Areas of the gate/drain and gate/source gaps.
β_b, β_g, η_b, η_g	Diode coefficient and ideality factor (barrier and gate junctions).
β, W_B	Common emitter current gain and effective base width for the phototransistor.
Δ, Δ_i	Substrate/epi layer barrier thickness (dark and illuminated).
ϕ_b	Built in potential in a semiconductor junction.
G_{bar}	Barrier conductance.
I_{phgd}, I_{phgs}	Optically induced currents in the barrier on drain and source side.
I_{sb}, I_{sg}, J_{sb}, J_{sg}	Reverse saturation current and current density (barrier and gate junctions).
I_{dark}, g_m, V_p	Dark current, transconductance and pinchoff voltage for the MESFET.
R_g	External gate resistance.
ρ, G_{sub}	Substrate resistivity and conductance.
V_{ds}, V_{sg}	Drain to source and source to gate voltages.

Manuscript received June 5, 1990; revised January 21, 1992. This work was supported by the Stein Foundation, GE Aerospace Division, U.S. Army LABCOM ETDL and the Ben Franklin Partnership of the State of Pennsylvania.

A. Madjar and P. R. Herczfeld are with the Center for Microwave-Lightwave Engineering, Drexel University, Philadelphia, PA 19104.

A. Paolella is with the U.S. Army LABCOM, Electronics Technology & Devices Laboratory, Ft. Monmouth, NJ 07703.

IEEE Log Number 9200856.

I. Introduction

THE OPTICAL control of microwave devices and circuits, particularly MMIC's, has been attracting interest. The distribution of control signals to MMIC chips via

0018-9480/92$03.00 © 1992 IEEE

optical fibers, in place of metallic cables, can provide significant advantages, such as a reduction in size and weight, immunity to interference and good electrical isolation. However, p-i-n diodes, most commonly utilized in fiberoptic links, are not compatible with standard MMIC processing methods. The GaAs MESFET, the basic building block of MMIC's, can be used as a photodetector embedded on the monolithic chip itself, and thus serve as an optical input port. The MESFET as an optical port on MMIC's is the primary motivation for this study.

The photosensitivity of MESFET's were exploited in a significant number of investigations. De Salles *et al.* [1] reported the successful optical injection locking of MESFET oscillators. Herczfeld *et al.* [2] have demonstrated the optical control of gain and phase of an MMIC T/R module, using the MESFET as an optical detector. Paolella *et al.* [3, 5] and Herczfeld *et al.* [4] have used a similar approach to optically control an MMIC distributed amplifier, phase shifter of a T/R module and a switch. Rauscher *et al.* [6] have used a MESFET to simultaneously perform photodetection of a microwave modulated optical signal and to down-convert the detected signal to an IF frequency. This technique was also used to injection lock a 9.6 GHz MESFET oscillator to a bandwidth of 1.6 MHz [7]. In another experiment, Fetterman and Ni achieved beat frequencies up to 18 GHz by illuminating a MESFET with two lasers [8], and generated signals up to 52 GHz by superimposing an electrical RF signal to the gate [9].

The experimental and theoretical photoresponse of the MESFET has also been a subject of a number of studies. Simons *et al.* [10] reported the optical control of microwave and millimeter wave devices. They investigated the photovoltaic effect in the gate depletion region by approximating the photoinduced gate voltage. This work focused on the effect of biasing conditions and light intensity on the photoresponse. An experimental and theoretical MESFET characterization, with emphasis on the photovoltaic effect, was carried out by De Salles [11], [12]. He also investigated the photoresponse as a function of light intensity and performed a preliminary study of the backgating effect and optically induced substrate current. Darling [13] developed a perturbation analysis that accounts for the photoconductive effect under low level illumination. Madjar *et al.* [14] have identified photoavalanche effects in MESFET's, which can be utilized to increase the optical response. Mizuno [15] conducted an experimental study on dc optical response and microwave scattering parameters of the MESFET as function of the biasing conditions and light intensity. He concluded that the effect of the illumination on the device performance is similar to the control of the gate voltage. Gautier *et al.* [16] measured the effect of optical illumination on the MESFET both at dc and at microwave frequencies for several biasing conditions. They explain their results by the optically induced bias change (gate photovoltaic effect). Simons *et al.* [17] reported extensive measurements of the optical response of MESFET's and HEMT's both at dc and at microwave frequencies. They too attribute the device performance to the gate photovoltaic effect. Warren *et al.* [18] analyzed the optically controlled microwave MESFET oscillator. They represented the optical injection by an equivalent injection source at the device's gate. Papaionannou and Forrest [19] investigated the backgating and traps effect on the optical response of the MESFET. The traps cause a long tail in the response to a light pulse, and a slope smaller than 20 db/decade in the frequency response. The majority of these studies use various approximations to calculate the photovoltaic effect at the gate. Except for De Salles [11], [12], none of the above studies is based on the transport equations of the device, which link its performance to the physics. Therefore, there is a need for a more complete, in-depth study which relates the photoresponse to the physics of the device (e.g. doping levels, epilayer thickness), the biasing conditions as well as the characteristics of the optical input, namely the intensity and wavelength.

The objective of the work reported here is to develop a comprehensive model for the illuminated GaAs MESFET. The model should yield a better understanding of the operation of the device and provide an insight on how one might optimize its performance. The important features of the proposed model are:

1. The device is operated in any desirable biasing mode (active or beyond pinchoff).
2. The optical input, intensity and wavelength of the illumination, is accounted for explicitly.
3. The analysis is based on basic principles; the components of the optically induced current are derived from the differential equations governing the charge carrier transport.
4. The internal photovoltaic effect, which is shown to be of great importance, is fully characterized for the first time.

The structure of the device analyzed is outlined in Section II, and the theoretical device modelling is presented in Section III. Finally, simulation and experimental results are discussed in Section IV.

II. Device Structure

A cross-sectional view of a typical device constructed on a semi-insulating substrate is depicted in Fig. 1(a). The n-type epi layer with a doping concentration of $\sim 10^{17}$ cm^{-3} is grown on top of the substrate. The bonding pads are on the substrate itself (not on the mesa), while the drain and source electrodes are deposited on top of the epi layer, forming ohmic contacts. The mesa is etched in the gate region to obtain the desired current, and the gate Schottky metalization is vacuum deposited. The commonly used notations for the various geometrical parameters and the reference coordinates are shown in Fig. 1(a). The top view of the device, which contains several gate fingers connected to a common gate pad, is shown in Fig. 1(b). The drain electrodes are connected to a drain pad;

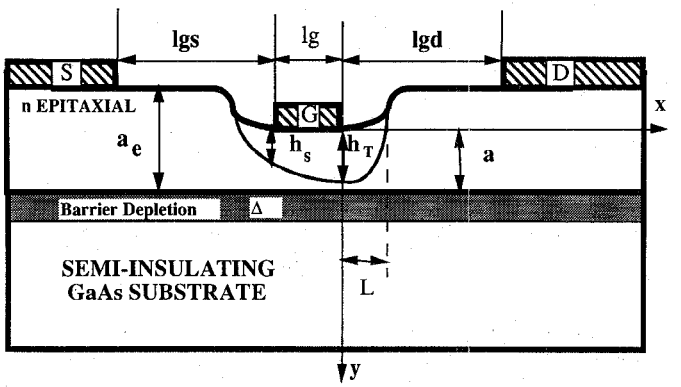

(a)

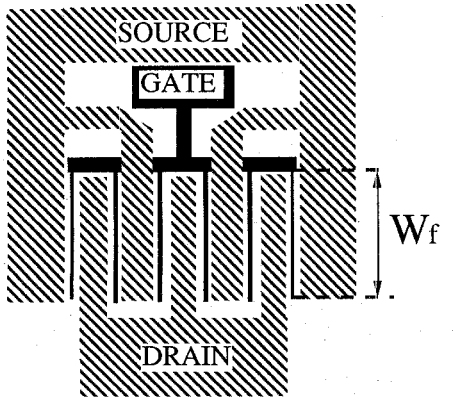

$W = W_f$ x (number of fingers)

(b)

Fig. 1. (a) Cross sectional view of the MESFET. (b) Top view of the MESFET.

the sources are connected by air bridges or by via holes to a common ground. Fig. 1(a) depicts also the depletion region between the epi layer and the substrate, a region which plays an important role in the optical detection mechanism in the MESFET.

III. Analysis

When the device is illuminated by light, which photon energy ($h\nu$) greater than the bandgap (1.41ev for GaAs), the absorbed photons generate electron-hole pairs resulting in excess current at the terminals. The analytic approach consists of solving the transport equation for the excess carrier densities subject to appropriate boundary conditions and then calculating the optically induced currents. However, due to the complex structure of the MESFET and because of the inhomogeneities caused by the optical absorption process, it is appropriate to divide the device into several sections, as shown in Fig. 2, and solve for it's contribution to the photoresponse. The five specific regions, depicted in Fig. 2, are related to different physical photoresponse mechanisms, the sum of which determines the overall response of the device to optical illumination. Region 1 is the illuminated segment of the gate depletion region—the carriers generated here contribute to the gate photocurrent. Region 2 is the illuminated section of the neutral channel—the optically generated carriers here contribute to the photoconductive current as well as to the gate current (via diffusion to the gate depletion region). Region 3 is the illuminated inter-electrode epi layer—here the excess carriers increase the conductivity, and thus reduce the parasitic resistances. Region 4 is the illuminated portion of the epi-substrate barrier—the carriers generated here establish a photocurrent between the epi layer and the substrate, which reduces the barrier height (internal photovoltaic effect). Region 5 is the illuminated part of the substrate—the carriers generated here contribute to the substrate current. The approach, based on the "dark" model of the MESFET developed by Chang and Day [20], will solve for the carrier density in each region.

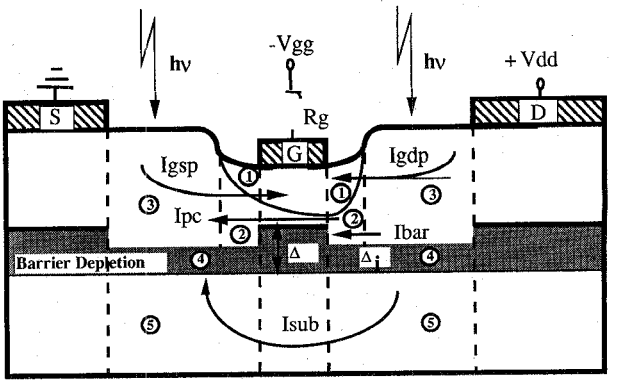

Fig. 2. Cross sectional view of MESFET demonstrating change of barrier under illumination.

The optical response of the MESFET, defined as the optically induced current measured at the drain, is the sum of four terms:

$$I_{\text{drain}p} = I_{pc} + I_{pvi} + I_{pvx} + I_{\text{leak}}$$

where I_{pc} is due to *photoconductive* effects in the channel, I_{leak} is the leakage current between the drain and source bonding pads, and I_{pvi} and I_{pvx} are caused by *internal* and *external* photovoltaic effects. The internal photovoltaic effect is related to the epi-substrate barrier, which is modulated by the light, and the source of the external photovoltaic effect is the gate junction. The currents due to the photovoltaic effects are further decomposed as follows: $I_{\text{pvi}} = I_{\text{bar}} + I_{\text{sub}}$ and $I_{\text{pvx}} = I_{\text{pvxr}} + I_{\text{gdp}}$, as shown in Fig. 2. Here I_{bar} is due to increase of the channel height by photo induced decrease of the epi-substrate barrier, I_{sub} is the substrate current due to the phototransistor effect, I_{gdp} is the contribution to the gate current from the drain side (this component flows via the drain), I_{pvxr} is the result of the external photovoltaic effect, when an external resistor is connected to the gate circuit.

Alternatively, the illuminated MESFET can be represented by the equivalent circuit, as shown in Fig. 3. Three optically induced current sources are noted. I_{dp}, the largest one, is the drain current source, which includes all the above mentioned drain current components except for I_{pvx}. The gate currents, I_{gdp} and I_{gsp}, are contributions from the

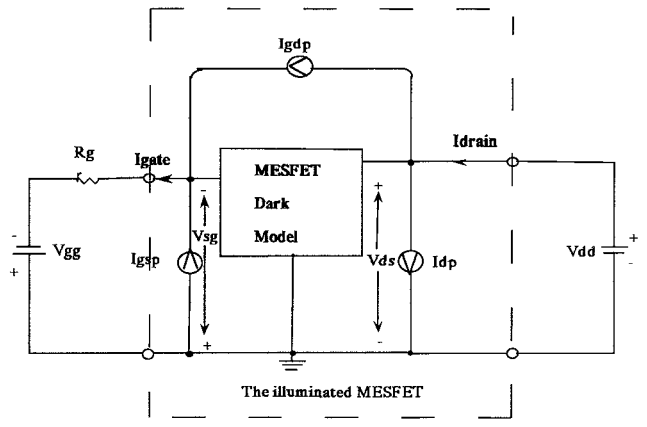

Fig. 3. Equivalent circuit for the illuminated MESFET.

drain and source sides of the gate junction, respectively. The total optically induced gate current, which is important for the gate photovoltaic effect, is defined as $I_{\text{gate}} = I_{\text{gdp}} + I_{\text{gsp}}$.

A. Photoconductive Current, I_{pc}

The photoconductive current density in the channel is defined in terms of the excess electron and hole distributions (derived in Appendix A): $J_{\text{pc}} = q(nv_n + pv_p)$. The corresponding current is calculated by integrating wJ_{pc} from $y = h_T$ to $y = a + \Delta - \Delta_i$ (see Figs. 1, 2):

$$I_{\text{pc}} = [qFA_{dL}(G_n + G_p)/((S^2 - 1)\cosh(h_{\text{cd}}/L_p))] \cdot \exp(-\alpha h_T)\{[S\sinh(h_{\text{cd}}/L_p) - \cosh(h_{\text{cd}}/L_p)] + \exp(-\alpha h_{\text{cd}})[\cosh(h_{\text{cd}}/L_p) - S^2(\cosh(h_{\text{cd}}/L_p) - 1)]\} \quad (1)$$

where $S = \alpha L_p$, $h_{\text{cd}} = a - h_T + \Delta - \Delta_i$. The drift velocities are calculated for the electric field value at $y = L/2$ (center of the illuminated depletion region extension on the drain side). The velocity relations for electrons is $v_n = \mu_n E$ for $E < E_c$ and $v_n = v_s + (v_{\text{pk}} - v_s)(E_c/E)^2$ if $E > E_c$. Similarly for holes we have $v_p = \mu_p E$ for $E < E_{\text{sp}}$ and $v_p = v_s$ if $E > E_{\text{sp}}$.

In GaAs the diffusion length is several microns (usually more than 10 microns), the channel height is in the submicron regime and the absorption coefficient is in the range $1\text{–}4 \times 10^6\ \text{m}^{-1}$ for wavelengths of interest (600–850 nm), therefore the following approximations are made: $h_{\text{cd}}/L_p \ll 1$, $S \gg 1$ and $\alpha h_{\text{cd}} < 1$. Using the Taylor expansion for sinh and cosh functions and for the exponential, the photoconductive current in the channel is approximated as

$$I_{\text{pc}} = 0.5qFA_{dL}(G_n + G_p)\exp(-\alpha h_T)\alpha L_p(h_{\text{cd}}/L_p)^3 \cdot \{1 - 0.5\alpha h_{\text{cd}}\} \quad (2)$$

It is noted that I_{pc} is a function of the bias conditions, the optical input (P_{opt}, λ) and the material and device parameters (w, τ_n, τ_p, a). Specifically, the photoconductive current, I_{pc}, decreases with V_{sg} (smaller h_{cd} and larger h_T), it is independent of V_{ds} (beyond the critical electric field for velocity saturation) and it intensifies with optical power density. Since the photoconductive current varies as the cube of the neutral channel height, which is extremely small (of the order of 0.1 micron), it may be negligible (submicro-amp range) for typical optical power densities.

B. Leakage Photocurrent, I_{leak}

The optical leakage current via the substrate is due to the photons absorbed between the drain and source bonding pads. In the regions where the pads are aligned opposite each other, a Schottky photodetector is created. The expression for the depletion region depth as well as its lateral extension is (Sze [21]):

$$d = \{2\epsilon(V_{\text{ds}} + \phi_b)/qn_s\}^{1/2} \quad (3)$$

The leakage current is obtained by integrating the generation rate, $\alpha F \exp(-\alpha y)$, in the entire volume of the depletion region:

$$I_{\text{leak}} = 2qFA_{\text{leak}}[1 - \exp(-\alpha d)] \quad (4)$$

The leakage photocurrent may be minimized by having the source and the drain bonding pads far apart and not facing each other (minimum w_s). Since A_{leak} is very small, the leakage current is negligible.

C. The Internal Photovoltaic Effect, V_{ph}

The current due to internal photovoltaic effect, $I_{\text{pvi}} = I_{\text{bar}} + I_{\text{sub}}$, is caused by the optically induced decrease in the potential barrier between the epitaxial layer and the semi-insulating substrate, as illustrated in Fig. 2 (the backgating effect). The difference in doping level between the epi layer and the substrate and subsequent diffusion of electrons from the epitaxial layer to the substrate gives rise to a potential barrier

$$V_{\text{bar}} = \eta_b(kT/q)\ln(n_e/n_s). \quad (5)$$

On the epi side, the space charge is created by the positively charged ionized donors, left behind by the migrating electrons. In this region the space charge is qn_e. On the substrate side, a negative charge distribution is established due to the electrons diffused from the epi which tend to concentrate close to the physical barrier, adjacent to the ionized donors. Therefore, it is assumed that the charge distribution is a delta function at the barrier.

The electric field distribution, shown in Fig. 4, and the voltage across the barrier is derived from Poisson's equation ($dE/dy = qn_e/\epsilon$):

$$V_{\text{bar}} = qn_e\,\Delta^2/(2\epsilon) \quad (6)$$

Alternatively we can solve for Δ

$$\Delta = [2\epsilon V_{\text{bar}}(qn_e)]^{1/2} \quad (7)$$

$\epsilon = \epsilon_0\epsilon_r$ is the dielectric permitivity of GaAs. The *dark* barrier width is obtained from (6). Under illumination the

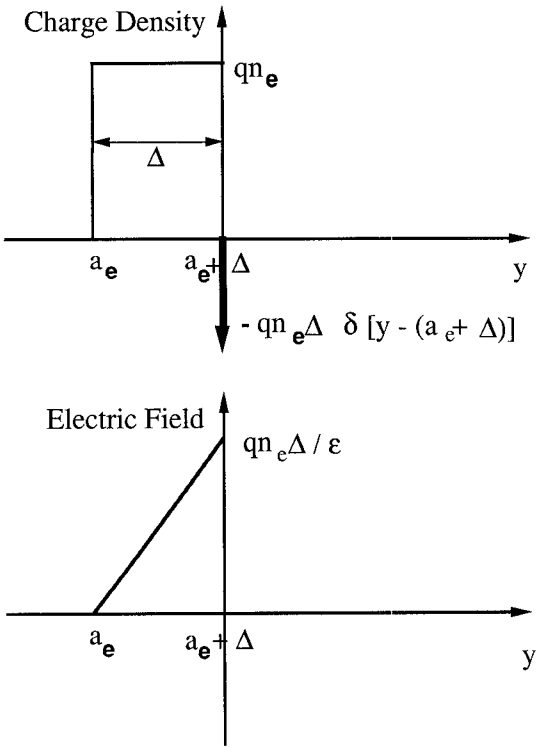

Fig. 4. Charge and electric field distribution in the epi/substrate barrier.

barrier potential as well as its width decrease in the illuminated region (see Fig. 2). The incident light generates electron-hole pairs in the depletion region of the barrier, and the electric field sweeps these carriers in opposing directions, establishing a current across the junction like in a Schottky barrier. Since the high-resistivity substrate is electrically in series with the junction, a photovoltage, V_{ph}, is generated, which is opposite the dark potential:

$$V_{ph} = V_{bar} - V_{bari} \tag{8}$$

From (6) and (7):

$$V_{bari} = qn_e \Delta_i^2/(2\epsilon) \quad \text{or} \quad \Delta_i = [2\epsilon V_{bari}/(qn_e)]^{1/2}. \tag{9}$$

The current in the junction is obtained by integrating the excess carrier density in the barrier region from $y = a_e + \Delta - \Delta_i$ to $y = a_e + \Delta$. On the drain side:

$$I_{phgd} = 2qA_dF \exp(-\alpha(a_e + \Delta))\{\exp(\alpha\Delta_i) - 1\}$$
$$\sim 2qA_dF \exp(-\alpha(a_e + \Delta))\alpha\,\Delta_i \tag{10a}$$

and on the source side:

$$I_{phgs} \sim 2qA_sF \exp(-\alpha(a_e + \Delta))\alpha\,\Delta_i \tag{10b}$$

In (10) the approximation $\exp(\alpha\,\Delta_i) \sim 1 + \alpha\,\Delta_i$ is used. The substrate resistance is calculated:

$$R_{sub} = \rho l_{sub}/[A_d + A_s] = l_{sub}/[qn_s\mu_s(A_d + A_s)]$$
$$= 1/[G_{sub}(A_d + A_s)]. \tag{11}$$

Kirchoff's Current Law yields the nonlinear equation for the photovoltage across the barrier:

$$V_{ph} = R_{sub}\{(I_{phgd} + I_{phgs}) - I_{sb}[\exp(\beta_b V_{ph}) - 1]\}$$
$$= R_{sub}(A_d + A_s)\{2qF \exp(-\alpha(a_e + \Delta))\,\alpha\,\Delta(1$$
$$- V_{ph}/V_{bar})^{1/2} - J_{sb}[\exp(\beta_b V_{ph}) - 1]\}. \tag{12}$$

In (12) we used the expressions from (10) and the relation $\Delta_i = \Delta(1 - V_{ph}/V_{bar})^{1/2}$, which evolves from (7), (8), and (9). Equation (12) can be solved by use of standard Newton-Raphson approach. Very important observation is that the *barrier photovoltage is independent of the biasing conditions*. It is noted that for the high-level illumination $V_{ph} \sim V_{bar}$, however for low-level illumination the barrier photovoltage is small, $V_{ph} \ll V_{bar}$, and $\exp(\beta_b V_{ph}) \sim 1 + \beta_b V_{ph}$. For low-level illumination (12) yields an analytic solution for the photovoltage:

$$V_{ph} = S_{opt}/[(G_{bar} + G_{sub}) + S_{opt}/(2V_{bar})] \tag{13}$$

where $G_{bar} = \beta_b J_{sb}$, G_{sub} is defined in (11) and $S_{opt} = 2q\,\Delta\alpha F \exp(-\alpha(a_e + \Delta))$ is the total optically generated charge of excess electrons and holes per unit area per unit time in the barrier depletion region assuming uniform generation rate as at the bottom of the barrier. For MMIC the typical doping level of the epi layer is $n_e \sim 2 \times 10^{17}$ cm^{-3}, therefore the maximum achievable V_{bar} is around 0.8 V. For *very* low level illumination the expression for V_{ph} is further reduced:

$$V_{ph} \sim S_{opt}/(G_{bar} + G_{sub}) \tag{14}$$

For high level illumination the exponential term dominates and (12) is approximated by neglecting the term V_{ph}. Thus:

$$V_{ph} = V_{bar}\{1 - [J_{sb}/S_{opt}]^2(n_e/n_s)^{(2V_{ph}/V_{bar})}\} \tag{15}$$

For very large S_{opt}, V_{ph} approaches V_{bar}, as expected.

To optimize the internal photovoltaic effect the optical input, S_{opt}, the barrier potential, V_{bar}, and the small signal slope of the photovoltage versus optical input have to be a maximum.

The optical input, S_{opt}, can be maximized by increasing the optical power level, P_{opt}, and by selecting the optimum wavelength for a given device (a_e). To attain the optimum wavelength the term $\alpha\lambda \exp(-\alpha(a_e + \Delta))$ needs to be maximized which is an easy task if the functional relation between α and λ is known. Measurements as well as calculations have shown that for GaAs MESFET's with relatively "thick" epi layers ($a_e \sim .4 - .5$ micron) the response rises for longer wavelengths, while for MESFETs with "thin" epi layer ($a_e < .2$ micron) the response falls with λ. This is consistent with large absorption of the photons at the epi-substrate barrier for both shallow and deep junctions.

To maximize barrier potential, the ratio n_e/n_s needs to be optimized. This can be achieved by using the best available semi-insulating substrate ($n_s \sim 10^7 - 10^8$ cm^{-3}). Finally, to maximize the slope in (14) the substrate conductance, G_{sub}, has to be minimized, which again requires reducing n_s as well as increasing the substrate thickness, l_{sub}.

D. Photocurrent Due to Channel Increase, I_{bar}

The decrease in the barrier height extends the channel in the illuminated region resulting in an increase of the drain current, I_{bar}. Since the channel height increases only in the illuminated region the exact calculation of the current is rather involved. De Salles [11], [12] showed that the optical drain current can be approximated by the difference of the dark drain current evaluated at source to gate voltages, V_{sg}, and $V_{sg} - V_{ph}$.

$$I_{bar} = I_{dark}|_{(V_{sg}-V_{ph})} - I_{dark}|_{V_{sg}} \sim g_m V_{ph}. \quad (16)$$

The optimum bias for the transconductance, g_m, depends on the doping profile of the active layer. For uniform doping, g_m is maximum at $V_{gs} \sim 0$. For nonuniform doping the optimal bias point must be determined empirically. Typically I_{bar} is in the milliamp range.

E. Substrate Photocurrent, I_{sub}

The optical current via the substrate under the barrier is accounted for by the phototransistor effect. In the absence of illumination the current in the substrate is negligible because the barrier prevents the electrons from entering into the substrate. Illumination, however, reduces the barrier, permitting the flow of electrons in the substrate. Disregarding the channel, the circumstance resembles a bipolar transistor with a "floating" base. The drain and source are analogous to the collector and emitter, respectively, and the substrate serves as the base. Because there is no base contact, the dark current via the substrate is negligible. The illumination produces two driving currents for the "transistor": 1) base-emitter junction current due to illumination of the source-gate gap. 2) base-collector junction current due to illumination of the drain-gate gap.

The equivalent circuit for this effective "bipolar transistor" with the driving current sources is depicted in Fig. 5. Kirchoff's Current Law yields the expression for the "collector" (i.e. substrate) current:

$$I_{sub} = (\beta + 1)I_{phgd} + \beta I_{phgs} \quad (17)$$

where β is the common emitter current gain of the "bipolar transistor" (Sze [21]):

$$\beta = 1/[\cosh(W_B/L_n) - 1] \quad (18)$$

The effective "base width", W_B, is estimated as the average distance of travel for the electrons from source to drain side in the substrate. Below pinchoff $W_B \sim (\pi/2)[l_g + .5(l_{gs} + l_{gd})]$, and beyond pinchoff $W_B \sim (\pi/2)[l_g + .5(l_{gs} + l_{gd} + L + h_s)]$. Equation (18) holds for V_{ds} values in the current saturation region of the dc curves. Inserting (11) into (18) we get:

$$I_{sub} = [(\beta + 1)A_d + \beta A_s](1 - V_{ph}/V_{bar})^{1/2} S_{opt}. \quad (19)$$

Clearly, to increase I_{sub} the inter-electrode gaps should be as large as possible so more photons can be absorbed. For low level illumination ($V_{ph} << V_{bar}$), I_{sub} is proportional to S_{opt}. For high level illumination:

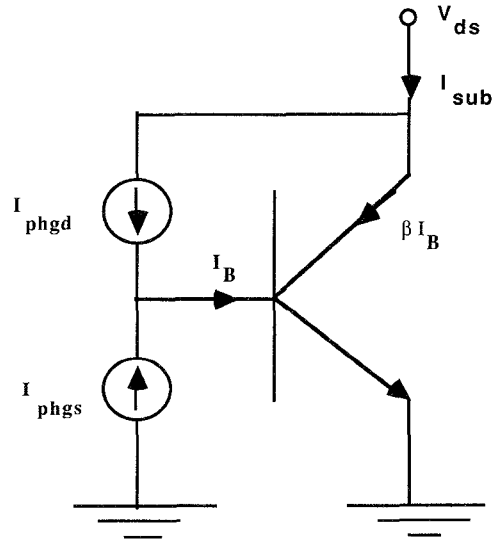

Fig. 5. Equivalent circuit for substrate photocurrent calculation.

$$I_{sub} = J_{sb}[(\beta + 1)A_d + \beta A_s](n_e/n_s)^{(V_{ph}/V_{bar})}. \quad (20)$$

The upper limit of I_{sub} is obtained as V_{ph} approaches V_{bar}. When the device is operated in the active region, I_{sub} is small compared to I_{bar}; however, near or beyond pinchoff I_{bar} approaches zero, and I_{sub} becomes dominant.

F. The External Photovoltaic Effect

The current due to the external photovoltaic effect, $I_{pvx} = I_{pvxr} + I_{gdp}$, is related to the photovoltage induced by the illumination at the gate when an external resistor (R_g) is inserted in the gate circuit.

G. Gate Photovoltage

The optical gate current in the external resistor produces photovoltage, which reduces the reverse bias across the gate-source junction, thereby indirectly increases the drain current. De Salles [11], [12] has shown that this effect can become the dominating contribution to the drain photocurrent. In fact, the photovoltage may drive the gate source junction into forward bias (around .4 v) accompanied by a large increase in drain current, because the channel height increases almost to its limit. The drain current in this case is calculated by first solving for the photovoltage, $V_{phx} = V_{sg|dartk} - V_{sg|ill}$ (the difference between the dark and illuminated source to gate voltage). From Fig. 3 Applying Kirchoff's Current Law to the gate node:

$$V_{phx} = R_g\{I_{gate} - I_{sg} \cdot [\exp(\beta_g(-V_{sg|dark} + V_{phx})) - 1]\} \quad (21)$$

where $V_{sg|dark} = V_{gg}$. Equation (21) can be solved for V_{phx} by the Newton–Raphson technique if an expression is provided for the gate current, I_{gate}. The value of V_{phx} is then used to calculate the drain current by utilizing the

"dark" model:

$$I_{\text{pvxr}} = I_{\text{dark}\,|\,V\text{sg}\,|\,\text{ill}} - I_{\text{dark}\,|\,V\text{sg}\,|\,\text{dark}} \sim g_m V_{\text{phx}}. \quad (22)$$

H. Gate Current

The derivation of the gate current on the drain and source side is patterned after the approach of De Salles [11], [12]. The current due to the holes generated in the depletion region is obtained by integrating the rate of optically generated holes ($\alpha F e^{-\alpha y}$) in the volume of the gate depletion region extending from $y = 0$ to $y = h_T$ on the drain side and from $y = 0$ to $y = h_s$ on the source side (see Fig. 1).

$$J_{\text{depd}} = qF[1 - \exp(-\alpha h_T)] \quad \text{and}$$

$$J_{\text{deps}} = qF[1 - \exp(-\alpha h_s)] \quad (23)$$

The second constituent of the gate current is derived from the hole distribution in the channel under the depletion region. The details of the derivation are given in Appendix A. Taking the derivative of the expression for the hole distribution (A2) [$J_{\text{epi}} = qD_p \,\mathrm{d}p/\mathrm{d}y$ at $y = h_T$ or $y = h_s$], one obtains:

$$J_{\text{epid}} = \{qSF \exp(-\alpha h_T)/[(S^2 - 1)\cosh(h_{\text{cd}}/L_p)]\} \cdot [S\{\cosh(h_{\text{cd}}/L_p) - \exp(-\alpha h_{\text{cd}})\} - \sinh(h_{\text{cd}}/L_p)]. \quad (24)$$

The equation for J_{epis} (source side) is identical to (24) with h_T replaced by h_s and h_{cd} replaced by h_{cs}. Noting, as before, that $h_{\text{cd}}/L_p \ll 1$, $S \gg 1$ and $\alpha h_{\text{cd}} < 1$, we can simplify (25):

$$J_{\text{epid}} = qSF(h_{\text{cd}}/L_p)\exp(-\alpha h_T)(1 - h_{\text{cd}}/2L_p) \quad \text{and}$$

$$J_{\text{epis}} = qSF(h_{\text{cs}}/L_p)\exp(-\alpha h_s)(1 - h_{\text{cs}}/2L_p) \quad (25)$$

where $h_{\text{cs}} = a - h_s + \Delta - \Delta_i$. The total gate current is obtained by integrating ($J_{\text{depd}} + J_{\text{deps}} + J_{\text{epid}} + J_{\text{epis}}$) over the effective illuminated area of the depletion region. On the drain side of the gate, the depletion region height, h_T, is assumed constant over the illuminated area. On the source side of the gate the depletion region height varies with the distance towards the source electrode. However, it may be approximated by the height of the depletion region at the source edge of the gate, $h_s = a[(V_{\text{sg}} + \phi_b)/V_p]^{1/2}$, where V_p is the pinchoff voltage. The lateral extension of the depletion region on the source side is approximately h_s, so that the illuminated area may be estimated as: $A_{dL} = wL$ on the drain side and $A_{sL} = wh_s$ on the source side, where, w is the total gate width and $L \sim a((V_{\text{sg}} + V_{\text{ds}} + \phi_b)/V_p)^{1/2}$, ϕ_b is the built-in potential of the gate Schottky barrier (0.8 v for GaAs). The final expression for the optically induced gate current is:

$$\begin{aligned} I_{\text{gate}} &= I_{\text{gdp}} + I_{\text{gsp}} \\ &= (J_{\text{depd}} + J_{\text{epid}})A_{dL} + (J_{\text{deps}} + J_{\text{epis}})A_{sL} \\ &= qF[(A_{dL} + A_{sL}) - A_{dL}\exp(-\alpha h_T)\{1 - \alpha h_{\text{cd}}\} \\ &\quad - A_{sL}\exp(-\alpha h_s)\{1 - \alpha h_{\text{cs}}\}] \end{aligned} \quad (26)$$

Several observations are warranted. First, since the variables L, h_T, h_s increase, and therefore h_{cd}, h_{cs} decrease, with the bias voltages (V_{sg}, V_{ds}), the gate current, I_{gate}, is a moderately increasing function of the bias. Second, I_{gate} increases with optical power. Finally, the wavelength dependence of I_{gate}, governed by the function $\lambda[1 - \exp(-\alpha h_{T(s)})\{1 - \alpha h_{\text{cd(cs)}}\}]$, is complicated and closely tied to the device parameters. The first two observations have been verified experimentally by several authors ([10]–[12]; [17]). Our calculations show that the gate current is small, in the microamp range; however, it can cause an appreciable change in the source to gate voltage if an external resistor is connected to the gate circuit, to yield a large optical response in the drain current.

I. Limiting Cases for the Gate Photovoltage

Two limiting cases, low and high level illuminations, are considered. Since the optical gate current, I_{gate}, is a weak function of the bias, V_{sg}, we approximate it with its pinchoff value, $I_{\text{gate}} = qF(A_{\text{dL}} + A_{\text{sL}})(1 - e^{-\alpha a})$. Now (22) takes the form:

$$V_{\text{phx}} = R_g\{qF(A_{dL} + A_{sL})(1 - e^{-\alpha a}) - I_{\text{sg}}[\exp(\beta_g(-V_{\text{sg}} + V_{\text{phx}})) - 1]\}. \quad (27)$$

For the low level illumination the gate junction is reversed biased and the exponential term becomes negligible:

$$V_{\text{phx}} = qR_gF(1 - e^{-\alpha a})[A_{dL} + A_{sL}]. \quad (28)$$

For the high level illumination condition, the gate junction is forward biased, and the current through it dominates:

$$V_{\text{phx}} = V_{\text{sg}} + (1/\beta_g)\ln[1 + qF(1 - e^{-\alpha a}) \cdot (A_{dL} + A_{sL})/I_{\text{sg}}]. \quad (29)$$

h_s and L are bias dependent and their expressions depend on the doping profile in the active layer (i.e. for uniform doping $h_s = a((V_{\text{sg}} + \phi_b)/V_p)^{1/2}$, $L \sim a((V_{\text{sg}} + V_{\text{ds}} + \phi_b)/V_p)^{1/2}$). The optimum wavelength is found by maximizing the term $\lambda(1 - e^{-\alpha a})$, which depends on the functional relation between α and λ.

J. Discussion of the Analytic Results

The analytical expressions for the optical response are sumarized in Table I, where V_{ph} and V_{phx} are the solutions to the nonlinear equations (12) and (21), respectively. The relative magnitudes of the different optically induced currents may be evaluated from the table. For a well designed MESFET $A_{\text{leak}} \sim 0$ and thus the leakage current, I_{leak}, is negligible. Numerical simulations have shown that in the absence of an external resistor at the gate, the internal photovoltaic effect, I_{pvi}, prevails, and with a resistor in the gate circuit the external photovoltaic effect, I_{pvxr}, becomes large and dominant. The ratio of the photoconductive to the gate/drain photocurrent, $I_{\text{pc}}/I_{\text{gdp}}$, is always smaller than 0.3 and for typical device parameters is of

TABLE I
EXPRESSIONS FOR THE COMPONENTS OF THE OPTICALLY INDUCED DRAIN CURRENT

Current	Phenomenon	Analytical Expression
I_{pc}	photoconductive	$0.5qFA_{dL}\exp(-\alpha h_T)(G_n + G_p)(h_{cd}/L_p)^3\alpha L_p(1 - 0.5\alpha h_{cd})$
I_{leak}	leakage	$2qFA_{leak}[1 - \exp(-\alpha d)]$
I_{sub}	int. photovoltaic	$2qF\exp(-\alpha(a_e + \Delta))[(\beta + 1)A_d + \beta A_s](1 - V_{ph}/V_{bar})^{1/2}\alpha\Delta$
I_{bar}	int. photovoltaic	$g_m V_{ph}$
I_{gdp}	ext. photovoltaic	$qFA_{dL}[1 - \exp(-\alpha h_T)(1 - \alpha h_{cd})]$
I_{pvxr}	ext. photovoltaic	$g_m V_{phx}$

the order of 10^{-2}. This implies that I_{pc} is not very significant. The ratio of the substrate to the gate/drain photocurrent, I_{sub}/I_{gdp} is generally greater than unity (except at extremelly high illumination). The largest current component in the absence of external gate resistor is due to the optically induced increase in the channel height, I_{bar}, which can be demonstrated by examining the ratio I_{bar}/I_{sub}. For very low level illumination, the ratio is greater than 177 (g_m/w). This ratio is zero beyond pinchoff ($g_m = 0$); however, within the active dynamic range using typical transconductance values for small signal MESFET's, the ratio is in the range 2×10^4. Since I_{bar} saturates faster than I_{sub}, for high level illumination the ratio I_{bar}/I_{sub} decreases, and evetualy I_{sub} exceeds I_{bar} (typically for $V_{ph}/V_{bar} > 0.6$).

In the presence of a gate resistor the external photovoltaic effect, I_{pvxr}, becomes sizable, and with increasing values of R_g it can exceed I_{bar}. The critical value of R_g can be calculated by equating $V_{phx} = V_{ph}$. The result is

$$R_{gcrit} = 1/(1/R_{gvLL} + G_f F) \tag{30}$$

where $R_{gvLL} = \{2\alpha\Delta\exp(-\alpha(a_e + \Delta)\}/\{(G_{bar} + G_{sub})(1 - \exp(-\alpha a))(A_{dL} + A_{sL})\}$ is the value of R_{gcrit} for very low level illumination and $G_f = q(1 - \exp(-\alpha a))(A_{dL} + A_{sL})/(2V_{bar})$.

In reference to the optimizing of the optical response, some general conclusions may be drawn. These are grouped into three categories: optical input, bias, and device specifics.

To optimize the *optical input* to the device, the effective coupling of the light into the device and its wavelength has to be determined. To increase the number of photons absorbed (electron-hole pairs generated), the following measures are required: i. apply the maximum available optical power, ii. maximize the inter-electrode areas A_d, A_s, (enhance the optical coupling) and iii. adjust the thickness of the passivation layer so that it will act as an antireflection coating. The optimum wavelength is determined by maximizing the function: *i.* $\alpha\lambda\exp(-\alpha(a_e + \Delta))$ for the internal photovoltaic effect ($R_g = 0$) and ii. $\lambda(1 - e^{-\alpha a})$ for the external photovoltaic effect. To optimize the *bias conditions* one has to: i. maximize the effective illuminated area of the gate depletion region by increasing L (large bias voltage V_{ds}), ii. choose the bias conditions to maximize g_m and iii. select large values for R_g to increase the external photovoltaic effect. *Device parameters* which have the most important effect on the response are: i. maximize n_e/n_s (best available S.I. substrate)—maximum V_{bar}. ii. minimize G_{sub} (maximum l_{sub} and minimum n_s) and iii. if the internal effect dominates choose small a_e—see S_{opt} expression—subject to the practical constraint $a_e >= a$.

IV. EXPERIMENTAL AND COMPUTER SIMULATION RESULTS

The theoretical model presented above serves as the basis for computer simulations. It predicts the photoresponse of the illuminated MESFET as a function of the biasing conditions (V_{sg}), the optical input (wavelength – λ, power density – P_{opt}), and the pertinent device parameters (e.g. doping level and thickness of the epitaxial layer).

To verify the theoretical model, experiments were conducted on various MESFET's fabricated by different MMIC suppliers. The present comparison pertains to measurements carried out on a FUJITSU FSX51X MESFET. We selected this particular device because it had the best available documentation by the manufacturer on the relevant device parameters. (A study comparing the optical response of alternate type of MESFETs will be submitted to publication in the near future). The FUJITSU device has a gate length of about 1 micron, total gate width of 300 microns (two fingers of 150 microns each), a pinchoff voltage of 1.5 V, I_{dss} of 50 mA, maximum transconductance of 45 mmho and its specified to operate up to 18 GHz. The device is built on a semi-insulating GaAs substrate on top of which a buffer layer and an active layer are epitaxially grown. The chip is passivated by a double layer of silicon nitride (~1500 A) and silicon dioxide (~7000 A). In all the measurements, the response is defined as the excess drain current under illumination, namely, the difference between the illuminated and dark drain currents.

Internal Photovoltaic Effect

The internal photovoltaic mechanism in the epi-substrate region, discussed in the theory, was verified by direct measurement of the photovoltage. The device was mounted in a test fixture with the back side of the substrate soldered to ground with the source and gate pads unconnected. The drain pad was wire bonded to an output port, and the voltage between the drain and ground was monitored. The device was illuminated and the response

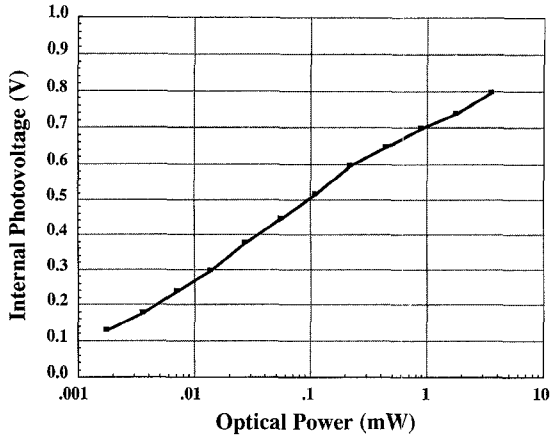

Fig. 6. Measured photovoltage at the epitaxial channel-substrate interface using an 850 nm laser as the illuminating source.

to the optical power was recorded. The photovoltage versus optical power intensity is depicted in Fig. 6. The drain to substrate photovoltage accross the epi-substrate barrier under open circuit conditions is somewhat larger than the photovoltage under normal operating conditions with the sources shorted to ground.

Photoresponse Versus Light Intensity

The photoresponse versus light intensity was measured by illuminating the MESFET with a semiconductor laser having a maximum output power of 3.5 mw at 850 nm. The light from the laser was passed through a variable optical attenuator and routed via an optical fiber (core diameter of 50 microns) to the MESFET by use of a micropositioner, which was situated to illuminate the entire active region of the device (approximately 100 microns in diameter). The measurement was performed for a fixed bias at about the center of the dynamic range (V_{sg} = 0.8 V, V_{ds} = 3 V) with R_g 0 and 1 MΩ; the results are shown in Fig. 7. The measured and calculated curves show excellent agreement. For R_g = 0 the internal photovoltaic effect dominates. For large values of R_g the external photovoltaic effect becomes the most vital term. The response is a monotonically increasing function of the optical power, however, the relation is not linear even for low optical power levels, as predicted by the analytic considerations.

Photoresponse Versus Wavelength

The output of a monochrometer operating in the range of 600 nm to 850 nm was used to illuminate the MESFET. The measured and simulated photoresponses are depicted in Fig. 8. The simulations were first carried assuming no passivation layer atop the device. These curves reflect the actual wavelength dependence of the device. The passivation layer acts as a filter with a periodic wavelength dependence, with transmission maxima at approximately 625 and 800 nm. The empirical curves show good agreement with the theoretical simulations. The somewhat lower response of the experimental results is attributed to photon absorption in the passivation layer.

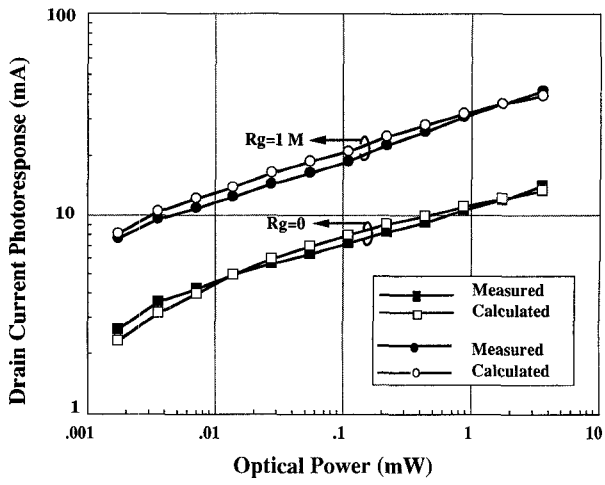

Fig. 7. Drain current photoresponse of the MESFET as a function of optical power for gate resistor values of 0 Ω and 1 MΩ. The MESFET was biased at V_{gs} = −0.8 V and V_{ds} = 3.0 V.

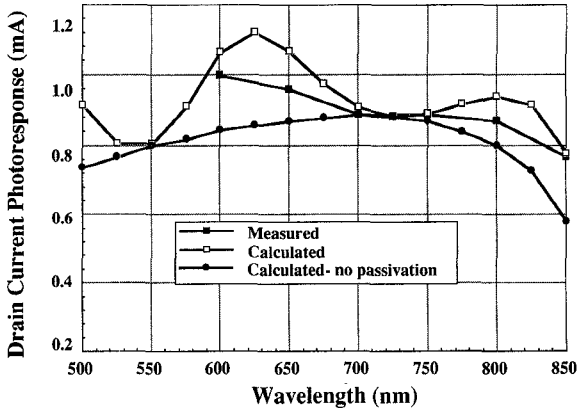

Fig. 8. Drain current photoresponse of the MESFET as a function of wavelength with 150 μW of optical power. The MESFET was biased at V_{gs} = −0.8 V and V_{ds} = 3.0 V.

Photoresponse Versus Bias

The dependence of the optical response on the bias was studied and the experimental and calculated results are shown in Fig. 9 for two wavelength values (600 and 850 nm). In these measurements V_{ds} was kept constant at 3 V since its effect on the response is negligible for values above the "knee" in the dc *I-V* curves of the device. Good agreement is demonstrated between the measured and calculated results. Fig. 9 includes also a plot of the transconductance, g_m, versus the source to gate voltage. As seen, the optical response tracks the general shape of g_m over most of the dynamic range. This implies, in accordance with the theory, that the principal optical detection mechanism in this case is the increase of the channel height due to the internal photovoltaic effect ($I_{bar} = g_m V_{ph}$, where V_{ph} is independent of the source to gate voltage). It is noted that the optical response deviates from the g_m curve at the edge of the dynamic range, near pinchoff and near zero source to gate voltage. The variance near pinchoff is due to the fact that for this bias I_{bar} is very small, comparable to the substrate current, I_{sub}, which does not depend on g_m. Furthermore, a small optical response is

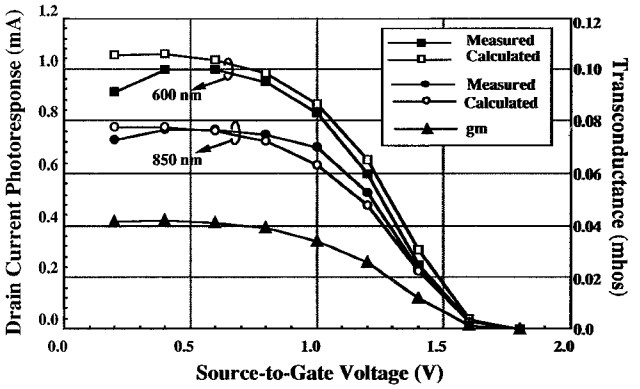

Fig. 9. Drain current photoresponse of the MESFET as a function of gate-to-source voltage at wavelengths of 600 nm and 850 nm. The MESFET was biased at $V_{ds} = 3.0$ V.

observed even beyond pinchoff (~ 1.5 V), which is attributed to I_{sub}. The decrease in the optical response as V_{sg} approaches zero, which is more pronounced for the shorter wavelengths at which the photons are absorbed near the surface, is due to a decrease in g_m as well as to surface states (which were not taken into account in this analysis).

V. Conclusions

A significant feature of the new analytical model of the optical response of a MMIC GaAs MESFET presented in this paper is the explicit dependence of the photoinduced current on the wavelength and intensity of the incident photon flux, under different biasing conditions. The model is also sensitive to pertinent device parameters. The investigation has shown that, in general, photovoltaic effects dominate the photoresponse. The internal photovoltaic effect, which has not been properly characterized in the past, is shown to be a major photodetection mechanism, and is incorporated in the modelling. Computer simulations based on the theory show good agreement with experimental results. Both theory and the experimental results suggest that the MESFET can be used as a monolithic photodetector comprising part of the MMIC chip, and serving as an optical control port. The analytic model can be considered as a tool to optimize the design and performance of optically controlled MMIC MESFET. Finally, although the present discourse is limited to the low frequency performance of the MESFET, the model, with suitable modifications, can be extended to the high frequency behavior of the device. These modifications are being carried out at the present time, and the results will be published in a future publication.

Appendix A

The distribution of the optically generated carriers in the channel is derived. For the MESFET, the channel is n type with relatively large doping, so the optically generated excess carrier distributions are governed by the minority carriers (holes). The differential equation for the holes is

$$D_p\, d^2p/dy^2 - p/\tau_p = -\alpha F \exp(-\alpha y) \qquad \text{(A1)}$$

where D_p is the hole diffusion coefficient. The boundary conditions are: $p = 0$ at $y = h_T$ (no carrier accumulation in the gate depletion region), $dp/dy = 0$ at $y = a + \Delta - \Delta_i$ (the holes generated in the epi/substrate depletion region are swept to the substrate by the electric field). Δ, Δ_i are the dark and illuminated barrier height, as shown in Fig. 2.

The solution to (A1) with the above boundary conditions is

$$\begin{aligned} p = p_{opt}\{&[\exp(-\alpha h_T)\cosh((a + \Delta - \Delta_i - y)/L_p) \\ &- \alpha L_p \exp(-\alpha(a + \Delta - \Delta_i)) \\ &\cdot \sinh((y - h_T)/L_p)]/ \\ &/\cosh((a + \Delta - \Delta_i - h_T)/L_p) \\ &- \exp(-\alpha y)\}/[(\alpha L_p)^2 - 1] \end{aligned} \qquad \text{(A2)}$$

where $p_{opt} = \alpha F \tau_p$ and $n = p\tau_n/\tau_p$, since the recombination rates of electrons and holes are equal. These expressions are used in the derivation of the gate current and photoconductive drain current.

Appendix B

The optical transmission coefficient from air into the active region of the device via the passivation layer (silicon nitride) is derived. The reflection coefficient at the GaAs-silicon nitride interface is:

$$\Gamma_L = (N_s - N_G)/(N_s + N_G) \qquad \text{(B1)}$$

where N_s, N_G are the refractive indices of silicon-nitride (2.05) and GaAs (3.5), respectively. At the air-silicon nitride interface, the reflection coefficient (normalized to the silicon nitride medium) is

$$\Gamma_{in|ns} = \Gamma_L \exp(-j2\theta) \qquad \text{(B2)}$$

where $\theta = 2\pi l N_s/\lambda$ is the electrical length of the silicon-nitride layer (l is the physical length). Finally, the reflection coefficient at the air-silicon nitride interface (normalized to air) is obtained from (B2):

$$\begin{aligned} \Gamma_{in} = &[(1 - N_s) + (1 + N_s)\Gamma_{in|ns}]/ \\ &[(1 + N_s) + (1 - N_s)\Gamma_{in|ns}] \end{aligned} \qquad \text{(B3)}$$

The transmission coefficient is: $T_r = 1 - |\Gamma_{in}|^2$. Its value for passivation layer thickness ranging from 0 to 0.2 microns varies from 0.7 to 1.0 and its dependence on the wavelength is moderate.

Acknowledgment

The authors thank Dr. A. Rothwarf for his comments and suggestions.

References

[1] A. A. De Salles, and J. R. Forrest, "Initial observations of optical injection locking of GaAs metal semiconductor field effect transistor

oscillators," *Appl. Phys. Lett.*, vol. 38, no. 5, pp. 392–394, Mar. 1981.
[2] P. R. Herczfeld *et al.*, "Optical phase and gain control of A GaAs MMIC transmit-receive Module," in *1989 IEEE MTT-S Int. Microwave Symp. Dig.*, May 1989.
[3] A. Paolella and P. R. Herczfeld, "Optical gain control of a GaAs MMIC distributed amplifier," *Microwave Optical Technology Lett.*, vol. 1, no. 1, pp. 13–16, Mar. 1988.
[4] P. R. Herczfeld, A. Paolella, A. Daryoush, A. Rosen, and W. Jemison, "Optical gain and phase control of a GaAs MMIC transmit-receive module," in *Proc. 1988 European Microwave Symp.*, September 12–16, 1988, Stockholm.
[5] A. Paollela, A. Madjar, P. R. Herczfeld, and D. Sturzebecher, "Optically controlled GaAs MMIC switch using A MESFET as an optical detector," in *1990 IEEE MTT-S Int. Microwave Symp. Dig.*, Dallas, May 1990.
[6] C. Rauscher, L. Goldberg, and S. Yurek, 'GaAs FET demodulator and down converter for optical-microwave links," *Electron. Lett.*, vol. 22, no. 13, pp. 705–706, June 19, 1986.
[7] L. Goldberg, C. Rauscher, J. F. Weller, and H. F. Taylor, "Optical injection locking of X-Band FET oscillator using coherent mixing of GaAlAs lasers," *Electron. Lett.*, vol. 19, no. 20, pp. 848–850, Sept. 1983.
[8] H. R. Fetterman and D. C. Ni, "Control of millimeter wave devices by optical mixing," *Microwave Optical Technology Lett.*, vol. 1, no. 1, pp. 34–39, Mar. 1988.
[9] D. C. Ni, H. Fetterman, and W. Chew, "Millimeter wave generation and characterization of a GaAs FET by optical mixing," *IEEE Trans. Microwave Theory Tech.*, vol. 38, no. 5, pp. 608–613, May 1990.
[10] R. N. Simons and K. B. Bashin, "Analysis of optically controlled microwave/millimeter-wave device structures," *IEEE Trans. Microwave Theory Tech.*, vol. MTT-34, no. 12, pp. 1349–1355, Dec. 1986.
[11] A. A. De Salles, "Optical control of GaAs MESFET's," *IEEE Trans. Microwave Theory Tech.*, vol. MTT-31, pp. 812–820, Oct. 1983.
[12] A. A. De Salles, "Optical control of microwave field effect transistors," Ph.D. dissertation, Univ. of London, 1982.
[13] R. B. Darling, "Transit-time photoconductivity in high-field FET channels," *IEEE Trans. Electron Devices*, vol. ED-34, 2, pp. 433–444, Feb. 1987.
[14] A. Madjar, A. Paollela, and P. R. Herczfeld, "Photo avalanche effects in A GaAS MESFET," *Microwave Optical Technology Lett.*, Feb. 1990.
[15] H. Mizuno, "Microwave characteristics of an optically controlled GaAs MESFET," *IEEE Trans. Microwave Theory Tech.*, vol. MTT-31, pp. 596–599, July 1983.
[16] J. L. Gautier *et al.*, "Optical effects on the static and dynamic characteristics of a GaAs MESFET," *IEEE Trans. Microwave Theory Tech.*, vol. MTT-33, Sept. 1985, pp. 819–822.
[17] R. N. Simons and K. B. Bhasin, "Microwave performance of an optically controlled AlGaAs/GaAs high electron mobility transistor and GaAs MESFET," in *IEEE MTT-S Int. Microwave Symp. Dig.*, June 1990.
[18] D. Warren *et al.*, "Simulation of optically injection-locked microwave oscillators using a novel SPICE model," *IEEE Trans. Microwave Theory Tech.*, vol. 36, pp. 1535–1539, Nov. 1988.
[19] G. Papaionannou and J. Forrest, "On the photoresponse of GaAs MESFETs: Backgating and deep trap effect," *IEEE Trans. Electron Devices*, vol. ED-33, no. 3, pp. 373–378, Mar. 1986.
[20] C. S. Chang and D. Y. S. Day, "Analytic theory for current-voltage characteristic and field distribution of GaAs MESFET's," *IEEE Trans. Electron Devices*, vol. 36, no. 2, Feb. 1989.
[21] S. M. Sze, *Physics of Semiconductor Devices*. New York: Wiley, 1981.

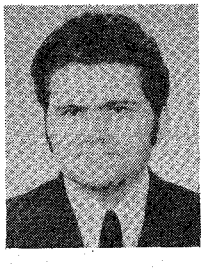

Asher Madjar (M'72-S'77-SM'83) received the B.Sc. and M.Sc. degrees from the Technion, Israel Institute of Technology, in 1967 and 1969, respectively, and the D.Sc. degree from Washington University, St. Louis, MO in 1979.

From 1969 to 1976 and from 1979 to 1989 he has been with RAFAEL, Haifa, Israel and with the Technion. In RAFAEL he performed research in the areas of passive and active microwave devices. He headed the MIC group from 1973 to 1976, served as a microwave Chief Engineer in the Communications Department from 1979 to 1982, and as Chief Scientist of the microwave Department from 1982 to 1989 with direct responsibility of the MMIC group from 1987 to 1989. In the Technion he taught several courses on Microwaves, Passive Microwave Devices, Active Microwave Devices, Transmission and reception Techniques, etc. and served as an instructor for graduate students. From 1989 to 1991 he was a visiting Professor at Drexel University in Philadelphia. During that time he performed research on optical control of microwave devices, and developed a comprehensive model for the optical response of the MESFET. He also participated in graduate students instruction and taught a course on microwave devices.

Dr. Madjar served as the Israel AP/MTT chapter chairman for several years, and in that capacity organized 11 symposia. From 1985 to 1989 he served as the secretary of the Israel Section of IEEE. He served on the technical committees for MELECON (1981), 14th, 15th, and 16th conventions of Electrical and Electronics Engineers in Israel. He is currently a member of the managing committee for the European Microwave Conference. He is the author or co-author of over 50 papers in the areas of microwave components and devices, MIC, MMIC, linear and non-linear microwave circuits (Harmonic Balance, APFT, etc.), microwave device modelling (including optical effects) and more.

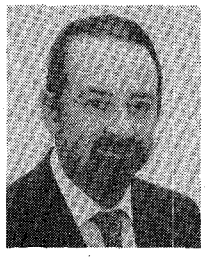

Peter R. Herczfeld (S'66-M'67-SM'89-F'91) was born in Budapest, Hungary in 1936 and is now a U.S. citizen. He received the B.S. degree in physics from Colorado State University in 1961, the M.S. in physics in 1963, and the Ph.D. in electrical engineering in 1967, both from the University of Minnesota.

Since 1967 he has been on the faculty of Drexel University, where he is a Professor of Electrical and Computer Engineering. He has taught 20 different courses at the graduate and undergraduate level, and lectured extensively in the U.S. and in ten other countries. He is known internationally as an expert in this field, having published over 250 papers in Solid-State Electronics, Microwaves, Photonics, Solar Energy, and Biomedical Engineering. In last three years alone, he has presented at least eight invited papers on the subjects related to this proposal, at IEEE-MTT, IEE-Antennas and Propagation Society, European Microwave Conference, Asia-Pacific Microwave conference, and SMBO conferences. Dr. Herczfeld is the Director of the Center for Microwave-Lightwave Engineering at Drexel, a Center of Excellence which conduct research in microwaves and photonics with over twelve U.S. corporations and government laboratories. He has directed more than fifty projects.

A member of APS, IEEE, SPIE, and the ISEC, he is a recipient of several research and publication awards, including the Microwave Prize. He has served as Guest Editor for a Special Issue of the IEEE TRANSACTIONS ON MICROWAVE THEORY AND TECHNIQUES and the *Journal of Lightwave Technology* on "The Application of Lightwave Technology of Microwave Devices, Circuits and Systems," and now is an Associate Editor for the *Microwave Journal*.

Arthur Paolella was born in Atlantic City, NJ in 1957. He received the Ph.D. degree in electrical engineering from Drexel University at the Center for Microwave/Lightwave Engineering in Philadelphia, PA in June 1992. He received the M.S. degree in electrical engineering from Fairleigh Dickinson University in 1985 and the B.S. degree in electronic engineering from Monmouth College in 1982.

He presently leads the Microwave Photonics Team within the Microwave/Lightwave Branch of the Electronics Technology and Devices Laboratory at Ft. Monmouth, NJ, where he is conducting research in the area of optical control of GaAs MMIC's, MESFET optical detectors, and in the development of analog microwave fiber optic links.

Dr. Paolella has authored or coauthored several publications on optical control of GaAs MMIC's and advanced mm-wave Gunn oscillators and has several patents.